

REGULAR PAPER

Underwater acoustic positioning in multipath environment using time-of-flight signal group and database matching

To cite this article: Tohru Yoshihara *et al* 2022 *Jpn. J. Appl. Phys.* **61** SG1075

View the [article online](#) for updates and enhancements.

You may also like

- [Application of 2E-2U method for free-field underwater calibrations of hydrophones and projectors in a reverberant laboratory test tank](#)
Ata Can Çorakç, Alper Biber, Talha Saydam *et al.*
- [Effect of Undersea Parameters on Reliability of Underwater Acoustic Sensor Network in Shallow Water](#)
N Padmavathy and Ch Venkateswara Rao
- [Performance of underwater source separation using narrowband and broadband signal at mini underwater test tank with varied in salinity and temperature](#)
B H Purwojatmiko, E Cahyaningtyas, D Arifianto *et al.*



Underwater acoustic positioning in multipath environment using time-of-flight signal group and database matching

Tohru Yoshihara¹, Tadashi Ebihara^{2*}, Koichi Mizutani², and Yuma Sato¹

¹Aomi Construction Co., Ltd., Chiyoda, Tokyo 101-0021, Japan

²Faculty of Engineering, Information and Systems, University of Tsukuba, Tsukuba, Ibaraki 305-8573, Japan

*E-mail: ebihara@iit.tsukuba.ac.jp

Received November 3, 2021; revised April 8, 2022; accepted April 24, 2022; published online June 10, 2022

One of the challenges in underwater acoustic positioning is the occurrence of missing measurements and large errors in multipath environments, such as shallow water and harbor areas. In this paper, we propose a new underwater positioning method for multipath environments by using direct wave arrival time groups and database matching. The proposed method accurately measures baseline length from the impulse response of the underwater channel by calculating time window groups that cover the propagation time from the sound source to each hydrophone in advance and then extracting only the impulse response around the propagation time of the direct waves when the sound source exists in a certain region of the measurement space. The performance of the proposed method was experimentally evaluated in a static environment. The results showed that the proposed method achieved an accuracy of 0.03 m and a precision of 0.02 m in a test tank. © 2022 The Japan Society of Applied Physics

1. Introduction

Acoustic positioning, which measures the positions of various devices operating in the sea where visibility is poor and electromagnetic waves are almost impenetrable, plays an extremely important role in ensuring accurate and efficient underwater operations and safety.¹⁻³ Acoustic positioning is performed by placing a sound source on an object (e.g. an underwater vehicle, an offshore structure, or a diver), receiving acoustic pulses from the source by a group of hydrophones whose coordinates are known, and measuring the baseline length between the source and the hydrophone or the direction of arrival of the sound waves. Acoustic positioning can be classified into three types according to the size of the baseline: super-short baseline (SSBL),⁴⁻⁶ short baseline (SBL),⁷⁻¹⁰ and long baseline (LBL).¹¹

The scope of this study is to establish a system to automatically measure the positions of construction machines underwater that are engaged in port and marine construction by utilizing information and communication technology. To achieve acoustic positioning at such construction sites, the following situations should be considered:

- (1) Port and marine construction sites are shallow and sometimes surrounded by quay walls, so the effects of a multipath environment are particularly apparent.
- (2) Normally, a construction machine is equipped with a pressure gauge, so its depth is known. In addition, barges and construction machines are wired to each other in order to synchronize the sending and receiving waves. Since the barge is the only offshore platform at the construction site, it is necessary to hang the hydrophone from the barge.

Figure 1 illustrates acoustic positioning at a port or marine construction site. Specifically, a signal is transmitted from a sound source located at an unknown coordinate (x_s, y_s, z_s) and received by a group of N hydrophones located at known coordinates (x_n, y_n, z_n) ($n = 0, 1, \dots, N-1$) ($N \geq 3$). The propagation time of the sound t_n from the source to each hydrophone $\#n$ is measured, and the baseline length between the source and each hydrophone l_n is calculated using the sound velocity and the sound propagation time t_n . The coordinates of the source (x_s, y_s, z_s) are then obtained by

solving simultaneous equations consisting of the unknown coordinates of the source, the known coordinates of each hydrophone, and the measured baseline lengths. To measure the sound propagation time t_n , the source emits a pulse-stretching signal such as a linear-frequency-modulated (LFM) chirp or an M-sequence-modulated signal, and pulse compression processes the signal that each hydrophone receives. This method is widely used to calculate the impulse response of an underwater channel.¹²⁻²⁴

One of the challenges in acoustic positioning is the occurrence of missing measurements and large errors in multipath environments. In a multipath environment, where multiple reflected waves exist in addition to the direct wave, the amplitude of a reflected wave may be larger than that of the direct wave due to interference between the reflected waves, as shown in Fig. 2. Therefore, if the signal with the largest amplitude among the channel impulse responses (CIRs) is assumed to be that of the direct wave, the baseline length cannot be calculated correctly, resulting in missing measurements and large errors. Hence, the academic question is how to separate a direct wave from a delayed wave using signal processing from CIRs in a multipath environment. In the field of underwater acoustic communication, measures against multipath environments have been widely considered.²⁵⁻⁵⁵ In the field of acoustic positioning, a few countermeasures have been considered. In one example, the positioning space is divided into meshes, precomputing the CIR for each mesh and storing it as a database (lookup table), and estimating the location of the sound source at the mesh by comparing the measured CIRs.^{56,57} In another example of a countermeasure, a window function for the CIR (e.g. existing acoustic releases such as 865 A and R12K, Teledyne Benthos) is set manually.

Inspired by those studies, in this paper we propose a new method for underwater positioning in multipath environments. The proposed method achieves positioning in two stages: rough positioning and precise positioning. In rough positioning, the proposed method divides the positioning space into meshes, precomputes the window function group that covers the propagation time of the direct wave for each mesh, stores the group as a database, and estimates the location of the sound source at the mesh by comparing the

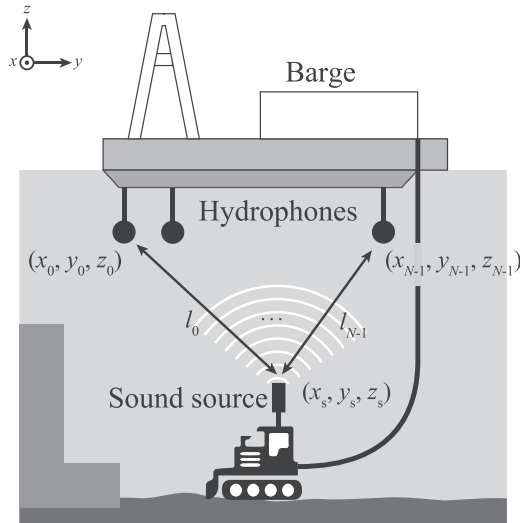


Fig. 1. Illustration of acoustic positioning by short baseline (SBL) (side view).

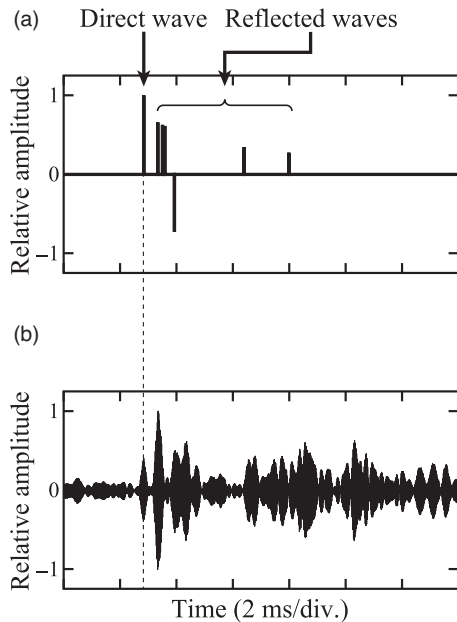


Fig. 2. Example of CIR in multipath environment; (a) calculated and (b) measured impulse responses.

measured CIRs.⁵⁸⁾ In precise positioning, the proposed method can set a window function for a CIR without knowing the location information in advance except for the depth of the transmitter and separates the direct wave from the delayed wave, resulting in precise measurement. If we can achieve an accuracy of 0.1 m in practical use, it will open

up new operational possibilities, such as unmanned marine construction. In Chap. 2, the principle of the proposed method is presented. In Chap. 3, the effectiveness of the proposed method is experimentally demonstrated and discussed. Chapter 4 is a summary of this work.

2. Acoustic positioning using time-of-flight signal blocks and database matching

2.1. Principle of the proposed method

In this subsection, we discuss the principle of the proposed method. For simplicity, we assume the following.

- The speed of sound in water c is known and constant.
- The depth of the sound source z_s is known.
- The coordinates of the hydrophones (x_n, y_n, z_n) are all known.
- There exists a line-of-sight link between the sound source and the hydrophone group.
- The transmitter system with the sound source and the receiver system with the hydrophone group are synchronized.

Figure 3 shows an overview of the proposed method. The method performs positioning as follows: (1) when a sound source exists in a certain region of the measurement space, the propagation time from the sound source to each hydrophone is calculated in advance, and a time window is calculated to extract only the signals around the propagation time. The time window groups (sets of time windows for all hydrophones when a sound source exists in a certain region of the measurement space) are then stored as a database for each region where the source exists. (2) Next, the impulse response group between the source and each hydrophone is actually measured. (3) Then, by comparing the impulse responses with the time window group, the area where the sound source exists is determined. (4) Using the windowed impulse responses between the sound source and each hydrophone, the coordinates of the sound source are calculated. The details of the proposed method are described below.

2.1.1. Rough positioning.

(1) Database construction

Consider a space of size $dJ \times dK$ ($0 \leq x \leq dJ, 0 \leq y \leq dK, z = z_s, d$ is a real number, and J and K are positive integers), as shown in Fig. 4. Assuming that the sound source exists in the mesh region $\#(j, k)$ $\{(j-1)d \leq \tilde{x}_j < jd, (k-1)d \leq \tilde{y}_k < kd \ (j=1, 2, \dots, J, k=1, 2, \dots, K)\}$ of size $d \times d$ in this space, we define the maximum and minimum times for the direct wave to propagate from the source to the hydrophone $\#n$ as shown in Eqs. (1) and (2),

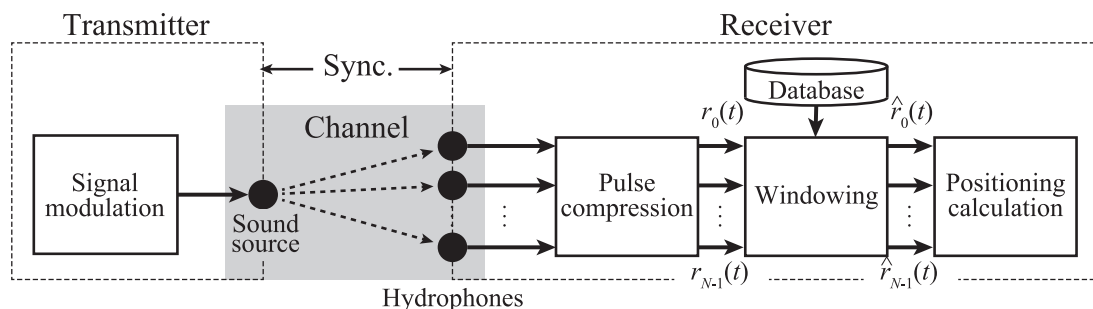


Fig. 3. Block diagram of acoustic positioning using time-of-flight signal blocks and database matching.

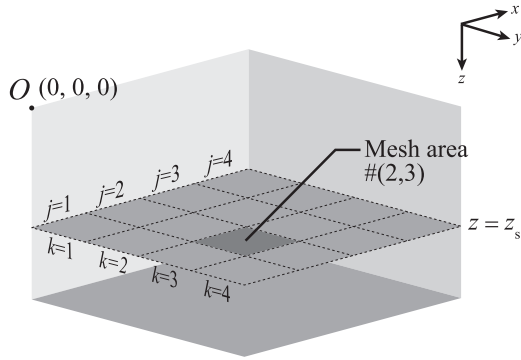


Fig. 4. Positioning area of size $dI \times dJ$ and mesh area of size $d \times d$.

respectively.

$$t_{\max}^{(j,k,n)} = (\max \sqrt{(x_n - \tilde{x}_j)^2 + (y_n - \tilde{y}_k)^2 + (z_n - z_s)^2}) / c, \quad (1)$$

$$t_{\min}^{(j,k,n)} = (\min \sqrt{(x_n - \tilde{x}_j)^2 + (y_n - \tilde{y}_k)^2 + (z_n - z_s)^2}) / c. \quad (2)$$

Then we define the window function $w^{(j,k,n)}(t)$ as the direct wave arrival time window in the mesh domain $\#(j, k)$, as shown in Eq. (3) and Fig. 5(a), and we calculate the group of window functions $w^{(j,k,n)}(t)$ for all j, k , and n and store them as a database, where

$$w^{(j,k,n)}(t) = \begin{cases} 1 & (t_{\min}^{(j,k,n)} \leq t \leq t_{\max}^{(j,k,n)}) \\ 0 & (\text{otherwise}) \end{cases}. \quad (3)$$

(2) Measurement of the impulse response group

The sound source emits pulse-stretching signals such

as LFM chirps and M-sequence-modulated signals, and pulse compression processes the signal received by each hydrophone to measure the impulse response $r_n(t)$ of the underwater channel [Fig. 5(b)].

(3) Comparison of impulse response group and time window group

The inner product of the impulse response group $r_n(t)$ and the window function group $w^{(j,k,n)}(t)$ is calculated for all j, k , and n [Fig. 5(c)]. Then, the mesh region $\#(j, k)$ with the largest inner product value is defined as the mesh region $\#(j_e, k_e)$ where the source exists as

$$(j_e, k_e) = \max_{j,k} \sum_{n=0}^{N-1} \left(\int r_n(t) w^{(j,k,n)}(t) dt \right). \quad (4)$$

2.1.2. Precise positioning.

(4) Positioning using a group of windowed impulse responses

The windowed impulse response $\hat{r}_n(t)$, which can be obtained by applying the window function group $w^{(j,k,n)}(t)$ at $j = j_e, k = k_e$ on the impulse response $r_n(t)$, is calculated for all n as,

$$\hat{r}_n(t) = r_n(t) w^{(j_e, k_e, n)}(t). \quad (5)$$

Then the sound propagation time t from the source to each hydrophone is measured, and the baseline length l_n is calculated using the sound velocity c and the sound propagation time by detecting the peak of the windowed impulse response as,

$$l_n = c \max_t \hat{r}_n(t). \quad (6)$$

Finally, the coordinates of the source (x_s, y_s, z_s) are estimated by solving the simultaneous equation using a nonlinear equations system (the Newton–Raphson method) as,

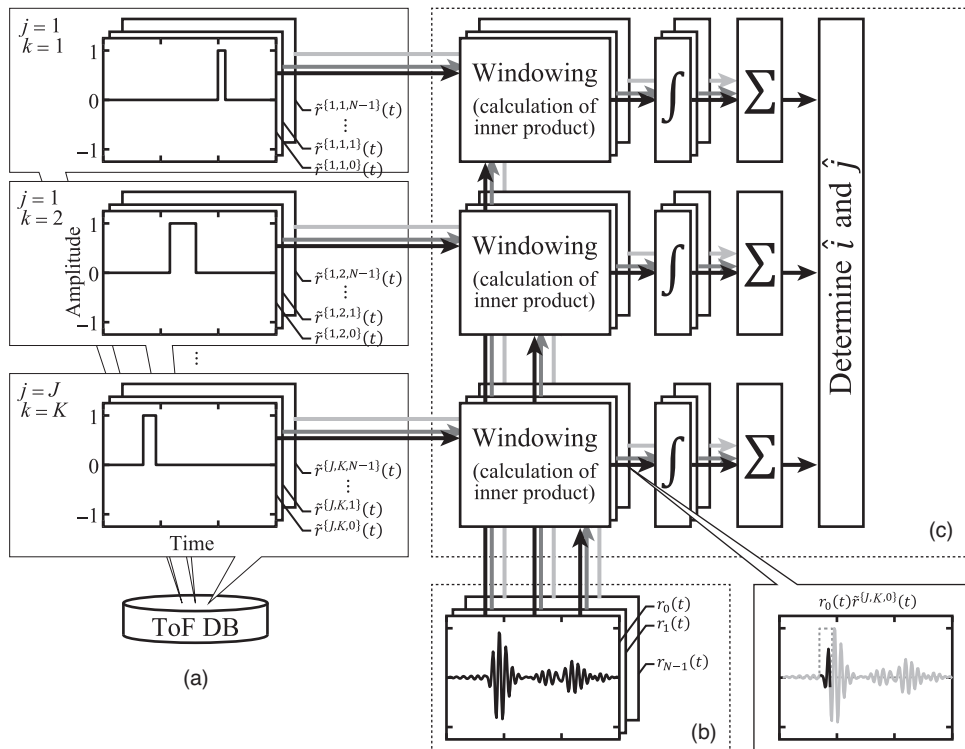


Fig. 5. Process of determining the area (rough positioning) where a sound source is located by comparing the impulse response group and the time window group.

$$\begin{cases} (x_s - x_0)^2 + (y_s - y_0)^2 + (z_s - z_0)^2 = l_0^2 \\ (x_s - x_1)^2 + (y_s - y_1)^2 + (z_s - z_1)^2 = l_1^2 \\ \vdots \\ (x_s - x_n)^2 + (y_s - y_n)^2 + (z_s - z_n)^2 = l_n^2 \end{cases} \quad (7)$$

Note that when solving the above equation using the Newton–Raphson method, it is necessary to set the initial value of the solution. In this paper, the initial value is the mesh coordinates calculated by Eq. (4).

2.2. Characteristics of the proposed method

We discuss the characteristics of the proposed method by describing the differences between it and the existing methods, as summarized in Table I. The proposed method (A) performs rough positioning by estimating the location of the sound source at the mesh using the database and (B) performs precise positioning by using a group of windowed impulse responses.

(A) Unlike the existing method, which performs rough positioning by comparing the measured and calculated CIRs,⁵⁶⁾ the proposed method compares the measured CIRs and the direct wave arrival time window. In the proposed method, this window exists area by area [Fig. 6(a)], while the calculated CIRs exist point by point in the existing method [Fig. 6(b)]. Hence, the accuracy of the rough positioning of the proposed method is expected to be exceeded that of the existing method if the size of the mesh area is properly selected. We would like to show that this assumption holds true in the following experiment. In addition, since the proposed method focuses only on the arrival time of direct waves, it does not require spatial information (which is necessary for the calculation of reflected waves) as long as the source and hydrophone groups can see each other.

(B) As for precise positioning, the proposed method is characterized by its ability to automatically apply the window function to a CIR, in contrast to the conventional method, which manually applies the window function to the CIR based on the rough location of the sound source. In the following experiments, we show that the proposed method can properly apply the window function to the CIR and can separate the direct and delayed waves in the time domain. In addition, there are several methods for signal processing after the window function is applied. In this study, the baseline length between the sound source and the hydrophone is calculated by detecting the peak of the signal after the window function is applied in the time domain. On the other hand, there exist several methods to calculate the position of a sound source, such as the multiple signal classification (MUSIC) method. In the following experiments, we also investigate signal processing after applying the window function and show that the most suitable method is the one that detects the peak of the signal with the window function

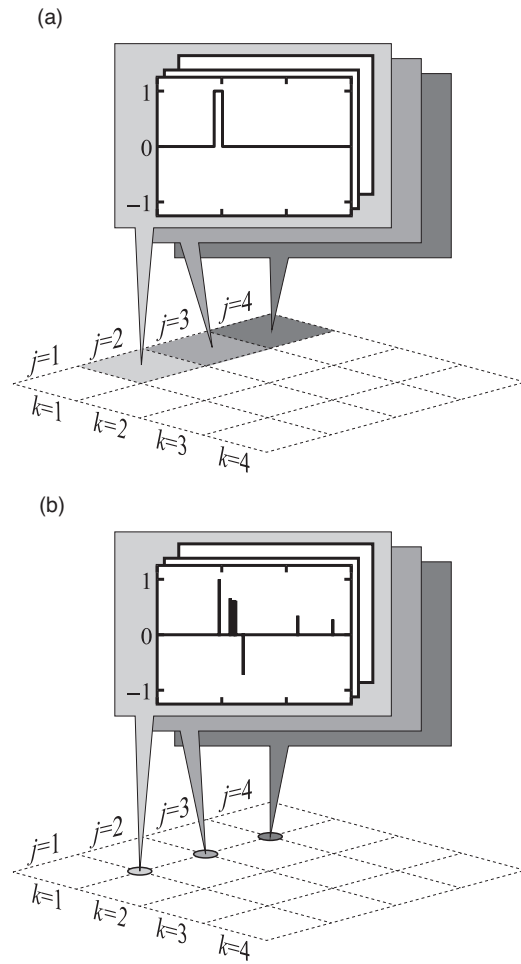


Fig. 6. Relationship between mesh area and (a) time window of the proposed method and (b) calculated CIRs of the existing method.

applied in the time domain and calculates the baseline length between the sound source and the hydrophone.

3. Experiments

3.1. Experimental environment

The performance of the proposed method in a static environment was evaluated by experiments. Figure 7 shows the experimental environment. Six hydrophones (BII-7523, Benthowave) were installed in a test tank of size 7.0 m × 9.0 m × 4.6 m at the positions indicated by the blue circles in the figure. A sound source (OST-2120, OKI Seatec) was also installed at the position indicated by the red circle in the figure, and its depth z_s was varied from 1.5 to 2.5 and 3.5 (m). The positions of the hydrophones and the sound source were set to simulate the acoustic positioning at the construction site, where the hydrophones are hung from the barge. A pulse-stretching signal was transmitted from the source, and the signal received by each hydrophone was

Table I. Comparison between proposed method and existing methods.

	Proposed method	Existing method ⁵⁶⁾	Existing method (acoustic release)
Rough positioning using database	✓ (Database: window)	✓ (Database: CIR)	N/A
Precise positioning using window	✓ (Required information in advance: depth of the transmitter)	N/A	✓ (Required information in advance: rough position and depth of the transmitter)

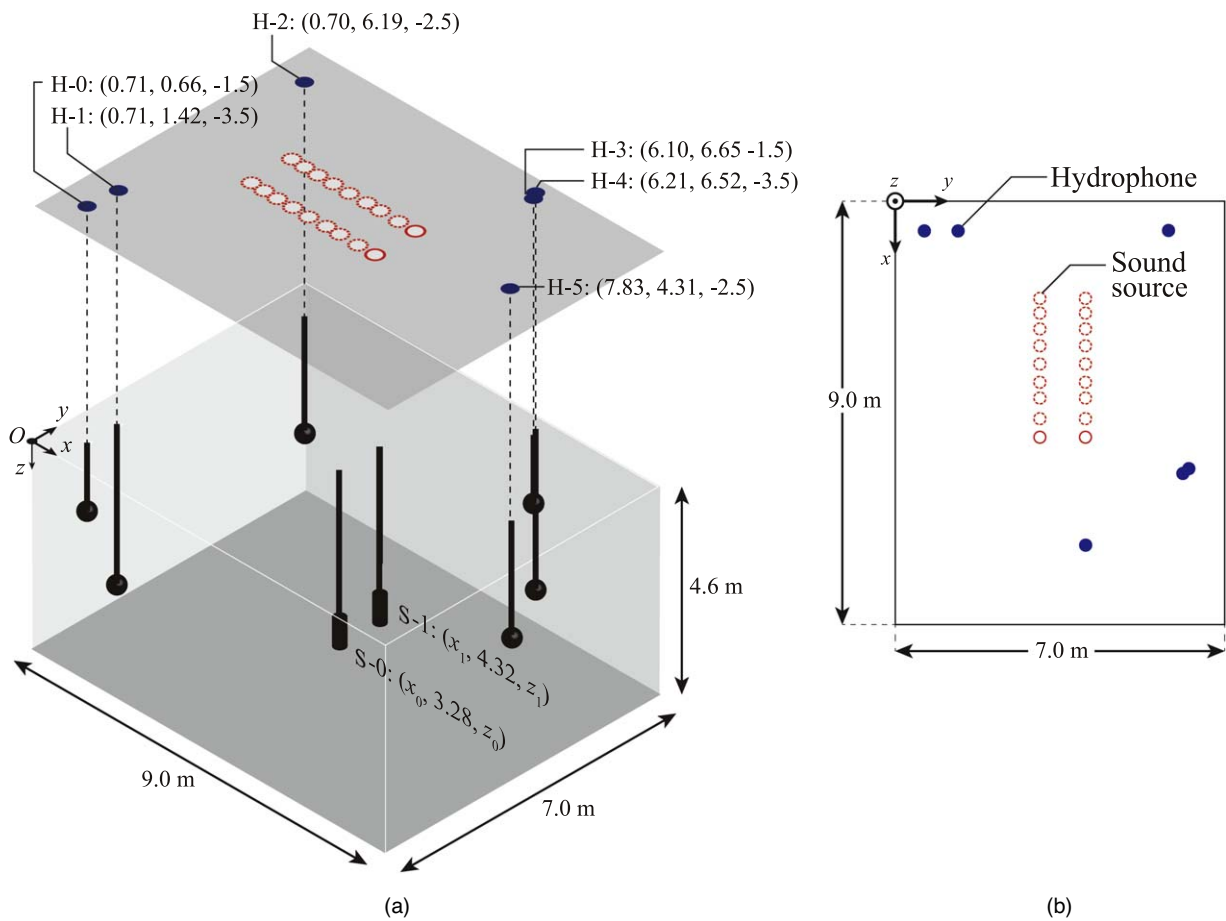


Fig. 7. (Color online) Experimental environment and placement of sound source (S) and hydrophone (H); (a) 3D view and (b) top view.

processed by pulse compression. A phase-shift modulated M-sequence (chip length: 127, center frequency: 35 kHz, bandwidth: 5 kHz, and time length: 25.4 ms) was used as the pulse-stretching signal. Note that the center frequency of the signal corresponds to the resonance frequency of the sound source, since we would like to emit the signal at the highest level possible, considering future experiments in actual seas. (Since offshore construction sites and the equipment deployed at them vary widely in size, it is necessary to increase the SPL in order to be able to perform positioning in noisy environments and over large areas). The sampling frequency of the signal f_s was 250 kHz. In the experiment, the sound pressure level was 178 dB (0 dB = $1 \mu\text{Pa V}^{-1}$ @ 1 m), the sound speed calculated from the water temperature was 1476 m s^{-1} , and the signal-to-noise ratio (SNR) was 41.6 dB. In addition, in this experiment the transmitter system and receiver system were connected by a wire and shared the same clock. Since the clock synchronization accuracy in this paper is sufficiently high, we did not consider the propagation of uncertainty from synchronization accuracy.

In this experiment, we performed (A) rough measurement and (B) precise measurement as follows. (A) In the rough measurement, the performance of the proposed method (using time windows) and that of the existing method (using calculated CIRs) were compared. Each calculated CIR contains the direct signal and an initial reflection signal. (B) In the precise measurement, the performance of the proposed method (in which baseline lengths are calculated by

detecting the peak of the signal after applying the window function in the time domain) and the existing MUSIC method were compared. We also performed positionings that did not consider a multipath environment, which (i) calculated the baseline length from the peak position of the CIR without windowing and (ii) performed CIR envelope detection and considered the earliest peak that exceeded the threshold (SNR > 20 dB) to be the direct wave. In both the rough and precise measurements, the accuracy (the difference between the measured average value and the true value) and the precision (the standard deviation of measured values) were used as evaluation indexes.

Although the MUSIC method is not effective for coherent multiple arriving waves, it can be applied if the time window is applied to eliminate delayed waves, since it deals with only direct waves. Therefore, the MUSIC method was applied to the separated direct wave by a time window. In addition, the steering vector was calculated using a spherical wave instead of a plane wave, based on the arrangement of the hydrophone in this experiment.⁵⁹⁾

3.2. Results and discussion

The experimental results are shown in Figs. 8–12. Let us first focus on (A) rough measurement. Figures 8(a-1) through 8(a-6) and 8(b-1) through 8(b-6) show examples of the impulse responses obtained in the experiment and time window group with the largest inner product value (proposed method, red line) and those obtained in the experiment and calculated CIRs with the largest inner product value (existing method, blue line) at each hydrophone, respectively, where $d =$

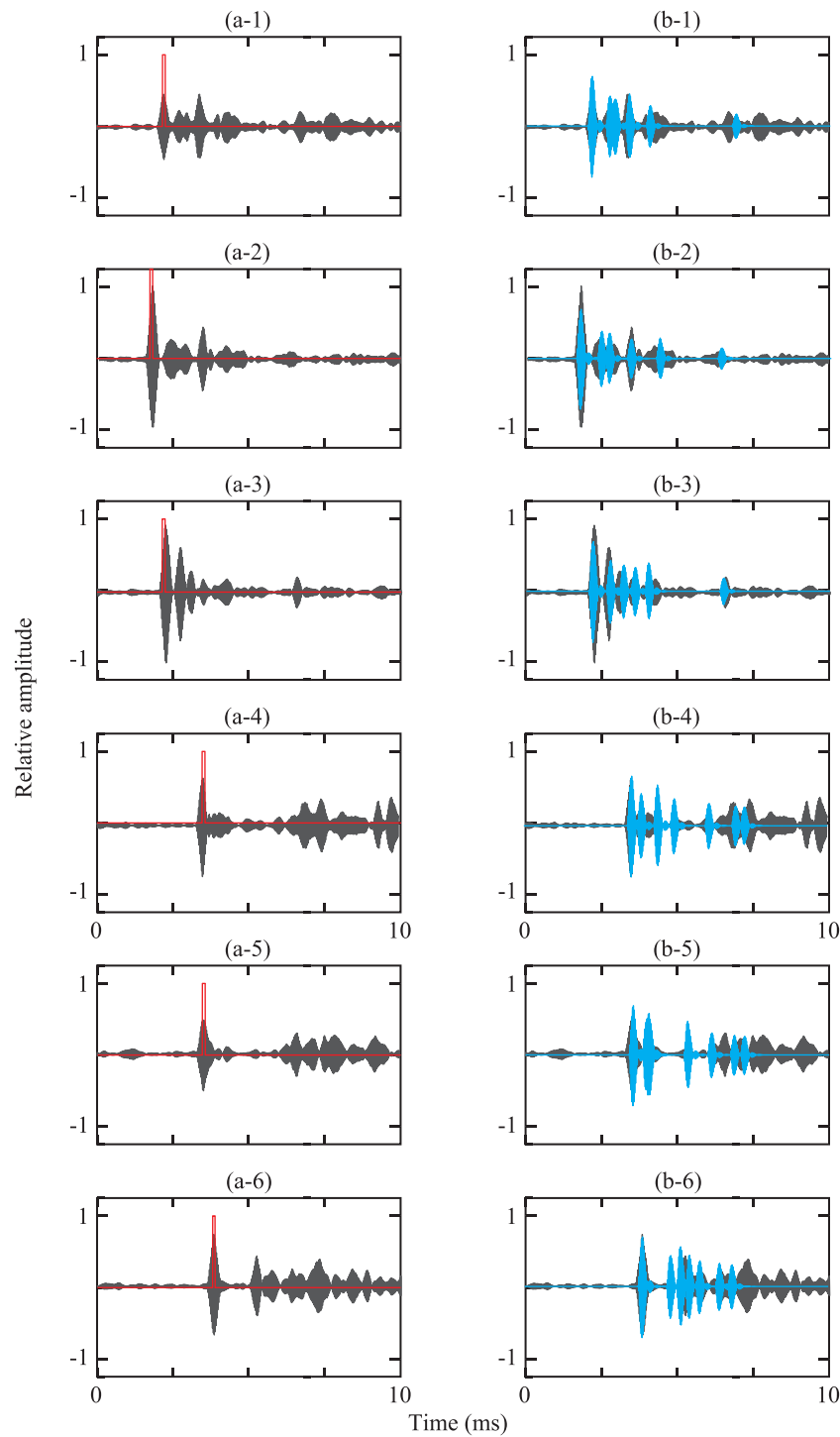


Fig. 8. (Color online) Examples of impulse responses obtained in the experiment; (a) with windows (proposed method, red line) and (b) calculated impulse responses (existing method, blue line).

0.1 (m). From the figure, we can confirm that the time window of the proposed method properly extracts the peak of the direct wave. On the other hand, the peak of the direct wave in the calculated CIRs and that in the measured CIRs are also consistent with each other in the existing method. Therefore, we decided to quantitatively analyze the accuracy of rough positioning using the proposed and existing methods.

Figure 9 shows a histogram of the rough positioning error (proposed method, red line; existing method, blue line) at various values of d . From this figure, we found that the use of the time window group (proposed method) outperforms the

use of calculated CIRs (existing method) in both accuracy and precision. One reason for this is thought to be that the direct wave arrival time window exists area by area in the proposed method [Fig. 6(a)], while the calculated CIRs exist point by point in the existing method [Fig. 6(b)], as discussed in Sect. 2.2. Hence, we found that the accuracy of the rough positioning of the proposed method can be improved by using the time window group instead of calculated CIRs.

In the rough measurement, the proposed method assumes that the time window groups are location-specific. In other words, if the time window groups have almost the same pattern in different locations, rough measurement cannot be

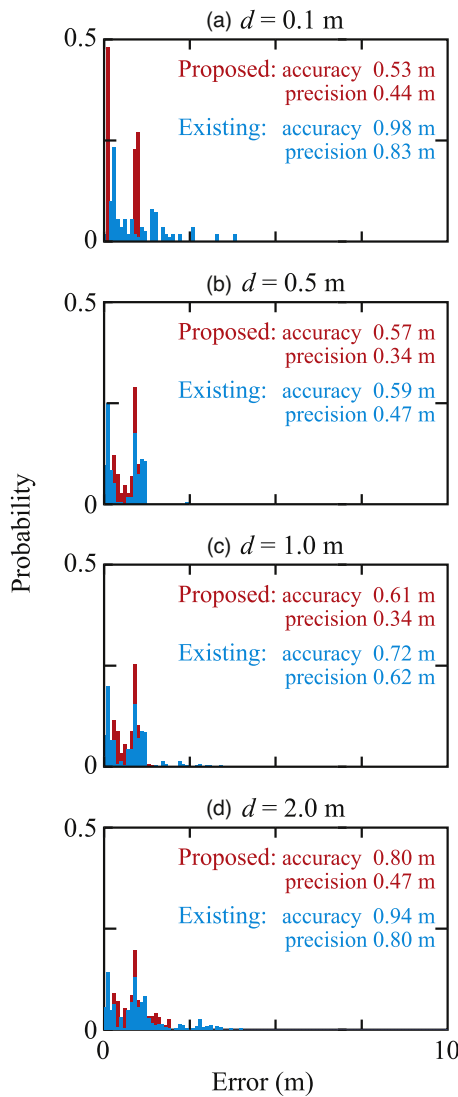


Fig. 9. (Color online) Histogram of rough positioning error; (a) $d = 0.1$ m, (b) $d = 0.5$ m, (c) $d = 1.0$ m, and (d) $d = 2.0$ m (proposed method, red line; existing method, blue line).

done accurately. Figure 10 shows a histogram of overlapping time among the time-window groups; the gray area indicates the overlapping time of the same time window groups. As the figure shows, the overlapping time and the probability that the time windows have almost the same pattern in different locations increase as the parameter d increases. Specifically, the probabilities are 0.1%, 0.8%, and 4.0% when d is 0.5 m, 1.0 m, and 2.0 m, respectively. From these results, we found that the time window group is sufficiently location-specific in this experimental condition when d is less than 1.0 m.

We next focus on (B) precise measurement. Figures 11(a-1) through 11(a-3) and 11(b-1) through 11(b-3) show the results of precise measurement using the proposed method (detecting the peak of the signal after applying the window function in the time domain) and the existing method (the MUSIC method is applied to the separated direct wave by a time window), respectively. As shown in Figs. 11(a-1) through 11(b-3), the proposed method outperforms the existing method; the accuracy and precision of the proposed method are 0.02, 0.03, and 0.08 (m) and 0.01, 0.02, and 0.13 (m) when $d = 0.1, 0.5,$ and 1.0 (m), respectively, while those of the existing method are 0.07,

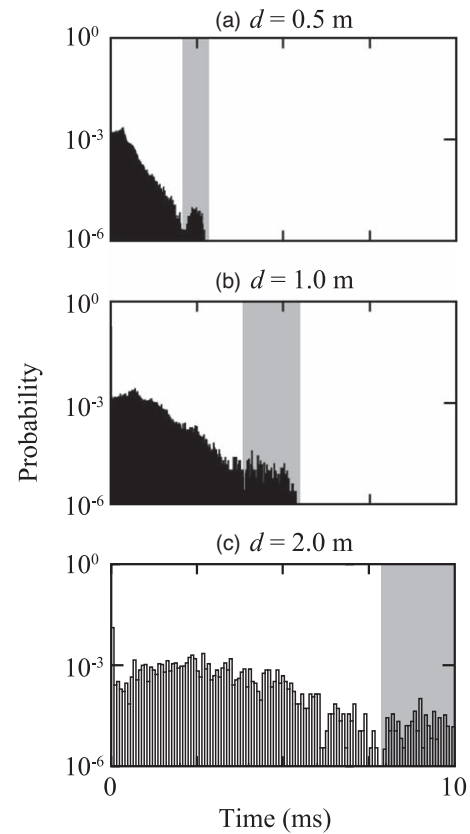


Fig. 10. Histogram of overlapping time among time window groups; (a) $d = 0.5$ m, (b) $d = 1.0$ m, and (c) $d = 2.0$ m; the gray area indicates the overlap time of the same time window group.

0.25, 0.52 (m) and 0.03, 0.11, and 0.27 (m), respectively. One reason why the proposed method outperforms the existing MUSIC method is thought to be that the MUSIC algorithm realizes maximum likelihood (ML) when the number of snapshots is large.⁶⁰⁾ However, as the number of d decreases, the number of snapshots becomes small since the number of sampling points decreases due to windowing, resulting in the decrease of accuracy. Specifically, the maximum numbers of snapshots (dc/f_s) are 16, 80, and 160 when $d = 0.1, 0.5,$ and 1.0 (m), respectively. On the other hand, as the number of d increases, the number of snapshots becomes large but unwanted signals such as reflected waves are also included, resulting in the decrease of accuracy. Hence, in precise measurement, the novelty lies in the detection of the direct wave propagation time using separated direct waves. Moreover, the classical method gave better results than the MUSIC method due to the limitation of the number of snapshots.

Let us also discuss the positioning accuracy of (B) precise measurement. In general, the positioning accuracy depends on the peak width of the correlation function with the signal frequency bandwidth and the phase of the carrier signal. The peak width of the correlation function in this experiment is 0.2 ms, which is about 0.3 m in terms of distance, and the resolution when the peak position is corrected by the phase of the carrier frequency is 0.02 ms, which corresponds to a resolution of about 0.04 m in terms of distance. From this point of view, it is clear that the accuracy and precision of the proposed method can achieve the order of resolution determined by the phase of the carrier signal under the conditions of $d = 0.1$ and 0.5 (m).

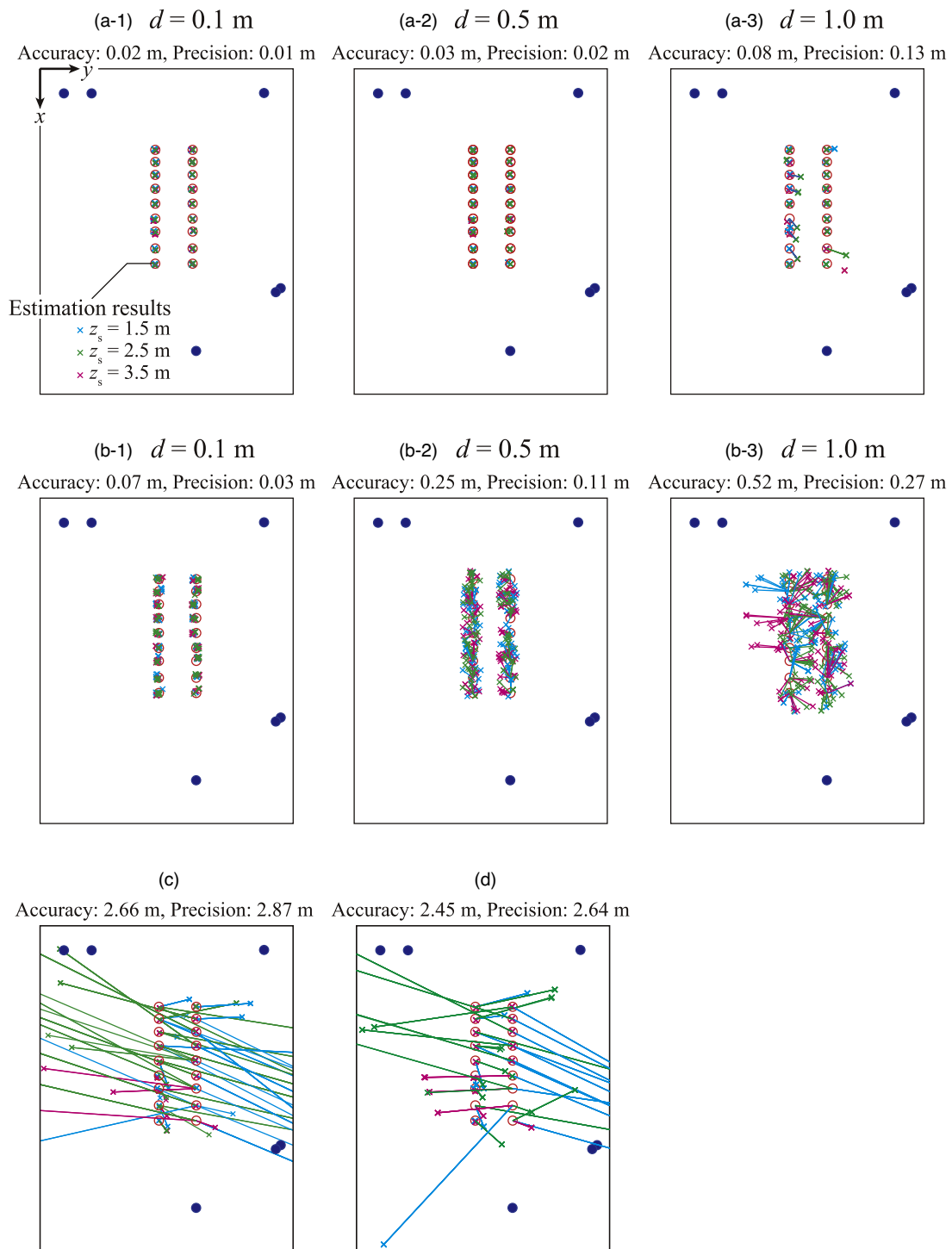


Fig. 11. (Color online) Experimental results of the proposed method when (a-1) $d = 0.1$ m, (a-2) $d = 0.5$ m, and (a-3) $d = 1.0$ m and of the MUSIC method when (b-1) $d = 0.1$ m, (b-2) $d = 0.5$ m, and (b-3) $d = 1.0$ m; and positioning methods that do not consider a multipath environment, where (c) calculates the baseline length from the peak position of the CIR without windowing and (d) performs CIR envelope detection and considers the earliest peak that exceeds the threshold to be the direct wave.

We also perform significant difference tests for which it is difficult to see obvious differences only in Fig. 11; proposed and MUSIC methods ($d = 0.1$ m) [Figs. 11(a-1) and 11(b-1)], and ($d = 0.5$ m) [Figs. 11(a-2) and 11(b-2)]. First, the results of the one-sample Kolmogorov–Smirnov test showed that there was no significant difference ($p < .05$) between the normal distribution and positioning error in the x and y directions for the proposed method and the MUSIC method,

for both $d = 0.1$ and 0.5 (m). Therefore, assuming that the positioning error follows the normal distribution, an F-test was conducted, and the results showed that there was a significant difference in variance between the proposed method and the MUSIC method ($p < .05$). Furthermore, Welch’s t-test results showed that there was no significant difference between the means of the proposed method and the MUSIC method for $d = 0.1$ m and a significant difference

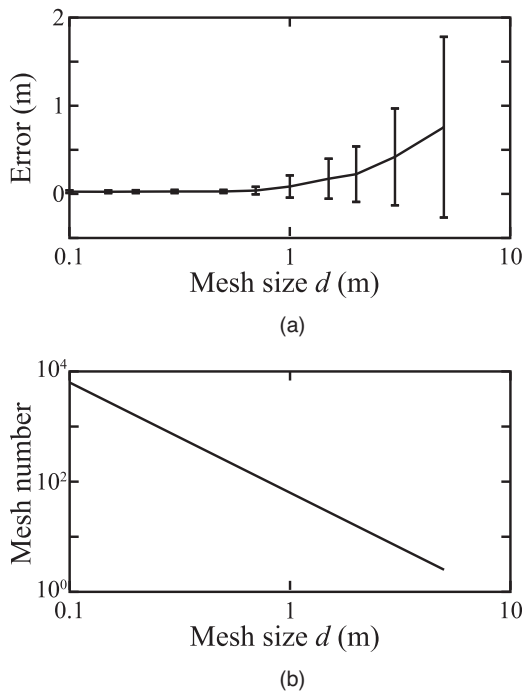


Fig. 12. Relationship between mesh size d and (a) measurement error and (b) mesh number in the proposed method.

for $d = 0.5$ m ($p < .05$). These results indicate that the proposed method has a significantly smaller standard deviation than the MUSIC method for both $d = 0.1$ and 0.5 (m), and the mean value of the error is also significantly smaller for $d = 0.5$ m.

As described in Sect. 3.1, in this experiment the transmitter system and receiver system were connected by a wire and shared the same clock. However, when each system uses a different clock, it is necessary to consider the propagation of errors due to the offset and skew of the clocks. Therefore, in the future it will be necessary to consider the effect of clock error propagation on positioning or to eliminate the effect of clock uncertainty by measuring the round-trip propagation time between the ocean and the seafloor, as in the case of transponders. Moreover, in this study we do not assume any motion of the receiver system. However, there is a possibility that a receiver system mounted to a barge will be subject to motion at actual construction sites. Since the motion of the barge will affect the positioning accuracy, it will be necessary to consider countermeasures.

We also show results of precise measurement that calculates the baseline length from the peak position of the CIR without windowing [Fig. 11(c)], performs CIR envelope detection, and considers the earliest peak that exceeds the threshold to be the direct wave [Fig. 11(d)]. As shown in Figs. 11(c) and 11(d), the accuracy and precision of the existing method without using the window function are 2.66 m and 2.87 m, respectively, whereas 2.45 m and 2.64 m are those of the existing method performing CIR envelope detection and considering the earliest peak that exceeds the threshold to be the direct wave. From these results, we found that the proposed method outperforms the existing methods and is suitable for underwater positioning.

Finally, we discuss the relationship between the size of the mesh area d and the accuracy and precision of the proposed method. Figure 10 shows the relationship between mesh size d and measurement error in the proposed method. As shown in the figure, the accuracy and precision are almost the same when d is less than 0.5 m, and both deteriorate when d is larger than 0.5 m in our experimental environment. As shown in Fig. 8(b), the number of mesh sizes increases as d becomes small, resulting in increased calculation cost. Hence, in this experimental environment, d of 0.5 m was found to be sufficient in both computational cost and accuracy, and it became clear that it is necessary to set an appropriate d depending on the environment.

4. Conclusions

A new underwater positioning method using a direct wave arrival time group and database matching is proposed for acoustic positioning in multipath environments, notably shallow water and harbor areas. The effectiveness of the proposed method in a static environment was evaluated experimentally, revealing that the proposed method has sufficient positioning accuracy, namely accuracy of 0.03 m and precision of 0.02 m, in a multipath environment (a test tank). In the future, we plan to apply this method to the positioning of moving objects and to verify its performance in actual seas.

Acknowledgments

This work was partly supported by JSPS KAKENHI Grant Number 19H02351.

- 1) M. Erol-Kantarch, H. T. Mouftah, and S. Oktug, *IEEE Commun. Mag.* **48**, 152 (2010).
- 2) H.-P. Tan, R. Diamant, W. K. G. Seah, and M. Waldmeyer, *Ocean Eng.* **38**, 1663 (2011).
- 3) L. Paull, S. Saeedi, M. Seto, and H. Li, *IEEE J. Ocean. Eng.* **39**, 131 (2014).
- 4) Y. Watanabe, H. Ochi, and T. Shimura, *Jpn. J. Appl. Phys.* **44**, 4717 (2005).
- 5) Y. Watanabe, H. Ochi, T. Shimura, and T. Hattori, *Jpn. J. Appl. Phys.* **48**, 07GL01 (2009).
- 6) Y. Watanabe, H. Ochi, T. Shimura, and T. Hattori, *Jpn. J. Appl. Phys.* **49**, 07HG13 (2010).
- 7) M. S. Sim, B.-K. Choi, B.-N. Kim, and K. K. Lee, *Jpn. J. Appl. Phys.* **55**, 07KG05 (2016).
- 8) S. M. Smith and D. Kronen, Proc. MTS/IEEE Oceans Conf., 1997, p. 714.
- 9) P.-P. J. Beaujean, A. I. Mohamed, and R. Warin, Proc. Europe Oceans Conf., 2005, p. 142.
- 10) H. Iwaya, K. Mizutani, T. Ebihara, and N. Wakatsuki, *Jpn. J. Appl. Phys.* **56**, 07JC07 (2017).
- 11) H. Iwaya, K. Mizutani, T. Ebihara, and N. Wakatsuki, *Jpn. J. Appl. Phys.* **57**, 07LC03 (2018).
- 12) K. Mizutani, N. Wakatsuki, and T. Ebihara, *Jpn. J. Appl. Phys.* **55**, 07KA02 (2016).
- 13) K.-C. Park, P.-H. Lee, and J. R. Yoon, *Jpn. J. Appl. Phys.* **51**, 07GG03 (2012).
- 14) K. Mizutani, S. Kawabe, I. Saito, and H. Masuyama, *Jpn. J. Appl. Phys.* **45**, 4516 (2006).
- 15) I. Saito, K. Mizutani, and N. Wakatsuki, *Jpn. J. Appl. Phys.* **46**, 4537 (2007).
- 16) Y. Katano, N. Wakatsuki, and K. Mizutani, *Jpn. J. Appl. Phys.* **48**, 07GB03 (2009).
- 17) I. Saito, K. Mizutani, N. Wakatsuki, and S. Kawabe, *Jpn. J. Appl. Phys.* **48**, 07GB05 (2009).
- 18) J. Igarashi, K. Mizutani, and N. Wakatsuki, *Jpn. J. Appl. Phys.* **49**, 07HC04 (2010).
- 19) I. Nishimura, M. Ishigamori, and A. Yamada, *Jpn. J. Appl. Phys.* **51**, 07GB13 (2012).

- 20) T. Motegi, K. Mizutani, and N. Wakatsuki, *Jpn. J. Appl. Phys.* **52**, 07HC05 (2013).
- 21) S. Hirata and H. Hachiya, *Jpn. J. Appl. Phys.* **52**, 07HC06 (2013).
- 22) K. Hoshiba, S. Hirata, and H. Hachiya, *Jpn. J. Appl. Phys.* **52**, 07HC15 (2013).
- 23) N. Thong-un, S. Hirata, and M. K. Kurosawa, *Jpn. J. Appl. Phys.* **54**, 07HC06 (2015).
- 24) Y. Ikari, S. Hirata, and H. Hachiya, *Jpn. J. Appl. Phys.* **54**, 07HC14 (2015).
- 25) M. Stojanovic, J. Catipovic, and J. G. Proakis, *J. Acoust. Soc. Am.* **94**, 1621 (1993).
- 26) M. Stojanovic, J. A. Catipovic, and J. G. Proakis, *IEEE J. Oceanic Eng.* **19**, 100 (1994).
- 27) M. Stojanovic, J. A. Catipovic, and J. G. Proakis, *J. Acoust. Soc. Am.* **98**, 961 (1995).
- 28) M. Stojanovic, J. G. Proakis, and J. A. Catipovic, *J. Acoust. Soc. Am.* **100**, 2213 (1996).
- 29) G. F. Edelmann, T. Akal, W. S. Hodgkiss, S. Kim, W. A. Kuperman, and H. C. Song, *IEEE J. Ocean. Eng.* **27**, 602 (2002).
- 30) H. Ochi, Y. Watanabe, and T. Shimura, *Jpn. J. Appl. Phys.* **43**, 3140 (2004).
- 31) Y. Watanabe and H. Ochi, *Jpn. J. Appl. Phys.* **43**, 3134 (2004).
- 32) H. Ochi, Y. Watanabe, and T. Shimura, *Jpn. J. Appl. Phys.* **44**, 4689 (2005).
- 33) T. Shimura, Y. Watanabe, and H. Ochi, *Jpn. J. Appl. Phys.* **44**, 4722 (2005).
- 34) H. C. Song, W. S. Hodgkiss, W. A. Kuperman, M. Stevenson, and T. Akal, *IEEE J. Ocean. Eng.* **31**, 487 (2006).
- 35) T. Shimura, H. Ochi, and Y. Watanabe, *Jpn. J. Appl. Phys.* **45**, 4847 (2006).
- 36) T. Shimura, H. Ochi, and Y. Watanabe, *Jpn. J. Appl. Phys.* **46**, 4956 (2007).
- 37) B. Li, S. Zhou, M. Stojanovic, L. Freitag, and P. Willett, *IEEE J. Ocean. Eng.* **33**, 198 (2008).
- 38) T. Shimura, H. Ochi, and Y. Watanabe, *Jpn. J. Appl. Phys.* **47**, 4360 (2008).
- 39) B. Li, J. Huang, S. Zhou, K. Ball, M. Stojanovic, L. Freitag, and P. Willett, *IEEE J. Ocean. Eng.* **34**, 634 (2009).
- 40) T. Shimura, H. Ochi, Y. Watanabe, and T. Hattori, *Jpn. J. Appl. Phys.* **48**, 07GL02 (2009).
- 41) T. Ebihara, K. Mizutani, and N. Wakatsuki, *Jpn. J. Appl. Phys.* **49**, 07HG09 (2010).
- 42) T. Shimura, H. Ochi, Y. Watanabe, and T. Hattori, *Jpn. J. Appl. Phys.* **49**, 07HG11 (2010).
- 43) T. Ebihara and K. Mizutani, *Jpn. J. Appl. Phys.* **50**, 07HG06 (2011).
- 44) T. Ebihara and K. Mizutani, *Jpn. J. Appl. Phys.* **51**, 07GG04 (2012).
- 45) T. Ebihara and K. Mizutani, *IEEE J. Ocean. Eng.* **39**, 47 (2014).
- 46) T. Ebihara, *Jpn. J. Appl. Phys.* **52**, 07HG04 (2013).
- 47) T. Ebihara, H. Ogasawara, and K. Mizutani, *J. Marine Acoust. Soc. Jpn.* **41**, 157 (2014).
- 48) T. Ebihara and G. Leus, *IEEE J. Oceanic Eng.* **41**, 408 (2015).
- 49) T. Ebihara, H. Ogasawara, and K. Mizutani, *Jpn. J. Appl. Phys.* **55**, 037301 (2016).
- 50) Y. Kida, T. Shimura, M. Deguchi, Y. Watanabe, H. Ochi, and K. Meguro, *Jpn. J. Appl. Phys.* **56**, 07JG04 (2017).
- 51) T. Ebihara, G. Leus, and H. Ogasawara, *Phys. Commun.* **27**, 24 (2018).
- 52) Y. Kida, M. Deguchi, and T. Shimura, *Jpn. J. Appl. Phys.* **57**, 07LG01 (2018).
- 53) T. Ebihara, H. Ogasawara, K. Mizutani, and N. Wakatsuki, *Jpn. J. Appl. Phys.* **58**, SGGF07 (2019).
- 54) T. Ebihara, H. Ogasawara, and G. Leus, *IEEE J. Ocean. Eng.* **45**, 1594 (2019).
- 55) Y. Tabata, T. Ebihara, H. Ogasawara, K. Mizutani, and N. Wakatsuki, *Jpn. J. Appl. Phys.* **59**, SKKF04 (2020).
- 56) L. Liao, Y. V. Zakharov, and P. D. Mitchell, *IEEE Access* **6**, 4297 (2018).
- 57) Z. Michalopoulou and P. Gerstoft, *IEEE J. Ocean. Eng.* **45**, 92 (2019).
- 58) T. Yoshihara, T. Ebihara, K. Mizutani, and Y. Sato, *Proc. Symp. Ultrason. Electron.*, 2021, 2E3-4.
- 59) T. Okamoto, R. Nishiura, and Y. Iwaya, *Acoust. Sci. Tech.* **28**, 181 (2007).
- 60) P. Batista, C. Silvestre, and P. Oliveira, *Proc. IFAC NOLCOS*, 2010, p. 302.